The IRM Quarterly

ISSN: 2152-1972

Winter 2011, Vol. 21 No. 4

Inside...
Visiting Fellow's Report 2

Interpretation of Low-Temperature Data Part V: The Magnetite Verwey Transition (Part B): Field-Cooling Effects on Stoichiometric Magnetite Below T_V

Mike Jackson, Julie Bowles, Subir Banerjee, IRM

This installment of the *IRM Quarterly* series on low-temperature data returns to our friend magnetite. The first magnetite article (*IRM Quarterly*, 20:4, Winter, 2011) focused on the history and initial observations of the magnetite Verwey transition (T_v~120 K), as well as the basic physics and crystallographic transformation at the transition and a quick overview of its effects on magnetic properties. In this issue, we focus on the behavior of magnetite at $T < T_v$, restricting our discussion to pure (stoichiometric) magnetite, and emphasizing the effects of magnetic fields applied while cooling through T_v. In the context of common experiments performed at the IRM, we will focus on the interrelated magnetic and crystallographic behavior of magnetite and as it passes through T_v in the presence or absence of magnetic fields.

Cation substitution, oxidation, stress, and pressure can have dramatic effects on the temperature and nature of the transition, and we will reserve discussion of these for a future article. We will also devote an entire future issue to low-temperature demagnetization of room-temperature remanences carried by magnetite.

Review of the nature of T_v and the low-temperature polymorph of magnetite

At temperatures above T_v, magnetite is a ferrimagnetic semiconductor, properties which are related to its inverse spinel structure, with the tetrahedral (A) sites occupied by ferrous ions, and the octahedral (B) sites containing both ferrous and ferric ions. The electrical conductivity arises mainly from "electron hopping" between the mixed-valence octahedral ions, and the spontaneous magnetization is due to antiferromagnetic coupling of the A and B sublattices. As discussed in the previous article, at the Verwey transition there is a large decrease in electrical conductivity (Verwey, 1939) due to a cessation in electron hopping. Spontaneous magnetization intensity changes only minimally if at all, but there is a dramatic increase in magnetocrystalline anisotropy related to a crystallographic change from cubic ($T > T_v$) to monoclinic ($T < T_v$). These interrelated effects have a dramatic impact on magnetic properties, with domain state and crystal orientation playing additional roles.

Figure 1. Magnetite octohedra from Cerro Huanaquino, Bolivia. Photo by Rob Lavinsky, iRocks.com (via Wikipedia Commons).

At $T > T_v$, magnetocrystalline anisotropy energy is at a minimum when magnetization is oriented along the <111> cubic body diagonal. However, for magnetite crystals that are not perfectly equant, shape anisotropy dominates so that the easy axis of magnetization prefers to lie in the direction of particle elongation. As T approaches T_v from above, the cubic magnetocrystalline anisotropy constants (K_1, K_2) both approach zero, and at ~130K, K_1 changes sign. At this isotropic point, the magnetocrystalline easy axis changes from <111> to <100>, but the crystal structure remains cubic until further cooling to T_v, where it becomes monoclinic.

The c-axis of the monoclinic phase is closely aligned with one of the <100> axes of the cubic phase, and the monoclinic a- and b- axes correspond to face-diagonal orientations of the cubic phase. There is a slight distortion of the cubic lattice, approximately equivalent to an elongation along the cubic <110>, and the monoclinic c axis makes an angle of about 0.23 degrees with the cubic <100>. In particles larger than a few microns, this spontaneous strain is relieved by the formation of twin domains, effectively monoclinic crystallites, each having its own crystallographic orientation with a c-axis along one of the original cube edges. The monoclinic a- b- and c- axes are respectively the hard, intermediate and easy magnetic axes. Because monoclinic magnetocrystalline

cont'd. on pg. 7...

Visiting Fellow's Report

Magnetic assemblage in sedimentary rocks from the thrust-and-fold belts in the Appalachians, West Virginia

Myriam Kars
Ecole Normale Supérieure, Paris / University of Pau, France
kars@geologie.ens.fr

Many paleomagnetic studies in the Appalachian belt revealed the occurrence of a pervasive Kiaman remagnetization [1]. However, the origin of this remagnetization is not fully understood. Hypotheses about burial [2] or fluid circulation [3] have been tested, without a unique answer. Here, I investigate the rock magnetic mineralogy of carbonates and claystones to provide additional constraints. With respect to burial indicators, a peak temperature >200°C can be inferred in the Devonian shales from vitrinite data (Ro>2%) and Conodont Alteration Index (CAI 3.5-4) [4]. This contradicts with fluid inclusion microthermometry which suggests a maximum burial temperature ~150°C for the Devonian shales [5-8]. It is known from the work of [9], later confirmed by other authors [10-12], that pyrrhotite develops at the expense of magnetite for temperatures >200°C. Thus, the identification of pyrrhotite may be a good test to provide burial constraints.

During my visit, I focused on low-temperature investigations and more particularly the occurrence of pyrrhotite through the identification of the Besnus transition at 32 K [13]. The studied sedimentary rocks are of Silurian to Carboniferous age and are both mainly limestones (section A, Silurian-Early Devonian) and claystones (section B, Early Devonian-Early Carboniferous). The limestones from section A recorded the Late Paleozoic Kiaman remagnetization which occurred during the folding event (Alleghanian orogeny) (see [1] for a review; [2]). The carrier of this remagnetization is magnetite with superparamagnetic (SP) to single domain (SD) size [14-15]. Section B included the high petroleum potential Marcellus Fm. which triggers a renewed interest in the Appalachians.

Magnetic properties

I performed low temperature measurements with a MPMS. In the sequence used, a small magnetic field of 5 µT is applied while cooling the RT-SIRM (Room Temperature – Saturation Isothermal Remanent Magnetization). I also ran FORCs (First-Order Reversal Curves) and hysteresis loops at room temperature with a VSM.

I identified three distinct magnetic signals called hereafter S1, S2 and S3. The S1 signal is shown in Figure 1A and represents about 36% of the analyzed samples. It is characterized by an increase of the RT-SIRM from 300 to 10 K, which is typical of goethite [16]. It may display the Verwey transition of magnetite (~120 K). The warming curve called ZFC (Zero Field Cooled) decays monotonically to ~150-170 K and then decreases very rapidly to ~200-250 K where a break in slope occurs. The remanence is then quasi-stable to 300 K. We suggest that this feature represents nanoparticles of goethite [17]. The FORC diagrams (Figure 1B) show that there is a soft non-interacting SD magnetic mineral with a low coercive field H_c (~10 mT). It is probably the authigenic SD magnetite responsible for the remagnetization. Hysteresis loops carried out on the samples indicate a mixture of different coercive/grain-size minerals (Figure 1C) as a result of the wasp-waisted shape of the curve. This wasp-waisted feature is characteristic of the remagnetized limestones in North America [14].

A second type of magnetic signal called S2 (3% of the studied samples) is only found in the limestones (Figure 2A). It is characteristic of micron pyrrhotite [18-19]. The FORC diagram (Figure 2B) shows the occurrence of a low-coercive SD mineral, similar to the S1 signal. It is probably magnetite. The S2 signal occurs near the Alleghanian Structural Front.

A third magnetic signal called S3 is found in the

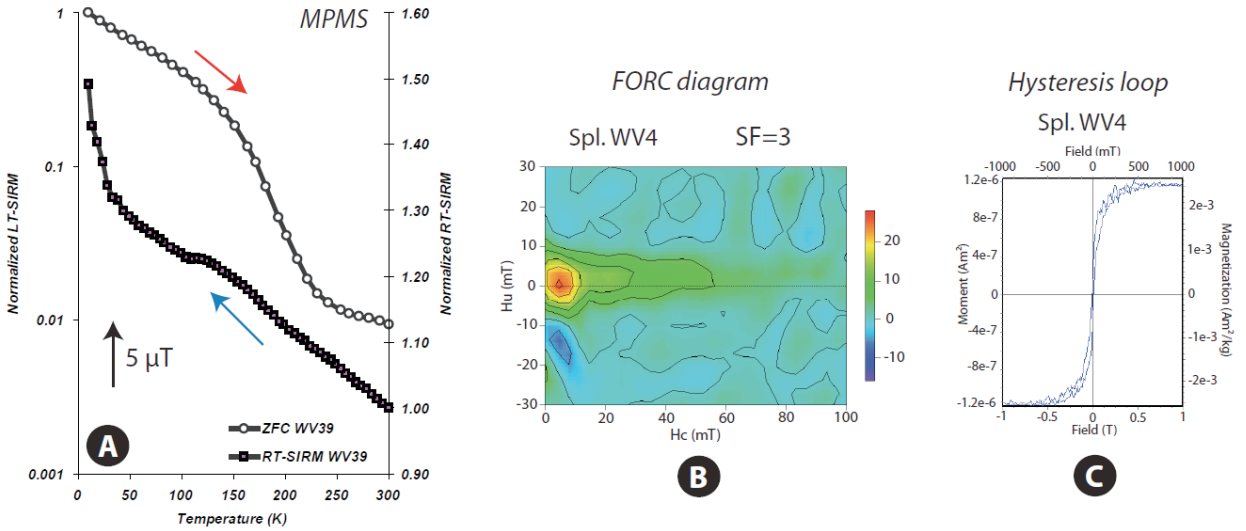

Figure 1. Magnetic signal S1: A) MPMS measurement, B) FORC diagram and C) hysteresis loop from the Tonoloway Formation (limestone from section A)

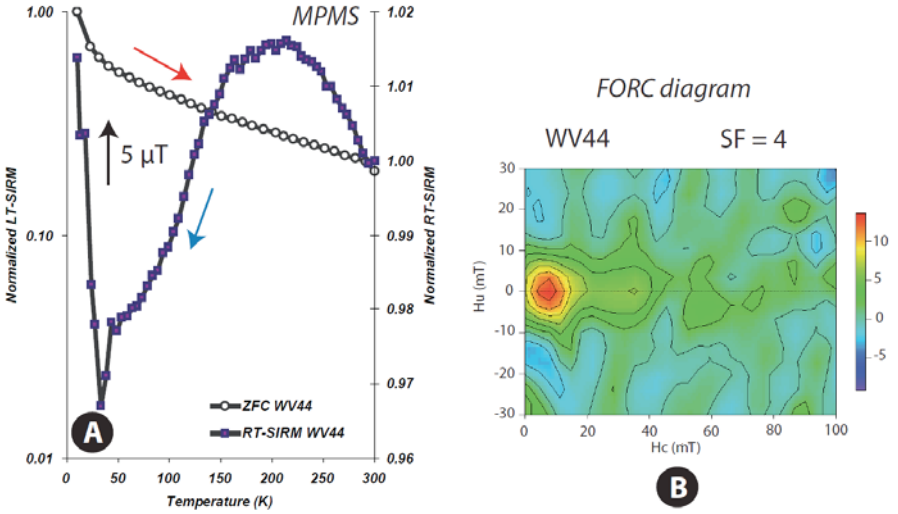

Figure 2. Magnetic signal S2: A) MPMS measurement and B) FORC diagram from Tonoloway Formation (limestone from section A)

claystones/siltstones (Figure 3). It represents the majority of the magnetic signals identified in the study area (44% of the studied samples). The S3 signal is characterized by a ZFC curve displaying a 2-step pattern as described by [20]. The drop of the remanence between 10 and ~35 K on the ZFC curve indicated the occurrence of SP grains. Both ZFC and RT-SIRM curves show the Verwey transition of stoichiometric SD magnetite. The increase of the magnetization from ~100 to 10 K on the RT-SIRM curve is called P-behavior and has a debated origin [21]. The room temperature hysteresis loops and FORC diagrams of samples displaying the S3 signal are poorly defined and hardly interpretable. This could be due to a higher paramagnetic input (e.g. clays) and a lower magnetization.

Magnetic assemblage and burial history

It appears from this study that the magnetic assemblages identified in the West Virginia samples are stratigraphically distributed, suggesting that lithologic or burial/thermal control may occur. The goethite-magnetite assemblage of S1 samples are situated mostly within the lower part of the stratigraphic section from the Tonoloway Formation to the Oriskany Sandstone (section A). The samples displaying the S3 signal are located in the upper part of the section from the Needmore Shale to the Chemung Group (section B). This stratigraphic distribution is probably influenced by lithologic parameters. Indeed, the section A is mainly limestones and the section B is mainly shales-siltstones.

The occurrence of neoformed stoichiometric magnetite and the absence of micron pyrrhotite in most collected samples lead to the fact that the rocks do not undergo burial temperatures higher than 200°C, except locally near the Alleghanian Structural Front [19,10]. The neoformed magnetite is the magnetic carrier of the widespread remagnetization of the Late Paleozoic sedimentary rocks in North America, recording the reverse Kiaman Superchron [1]. These observations and those from parallel studies lead us to propose a magnetic model of burial by recognizing characteristic magnetic minerals. A temperature range from ~50 to ~250°C is represented by neoformed magnetite. At temperatures higher than 250°C, micron pyrrhotite is the typical mineral [22]. Hence, the study of the magnetic assemblage of the Appalachians describes the "magnetite window" and the onset of the "pyrrhotite window".

The different magnetic assemblage may be also related to fluid circulation history, even if care was taken to sample away from the veins. Goethite, from section A samples, may be formed by oxidation of magnetite due to meteoric water circulation, as suggested by [8]. During uplift (post-folding event) breaching of folds by fracturing occurred. This allowed penetration of such oxidizing fluids in fracture zones. This magnetic assemblage would also correspond to burial temperatures > 110-120°C in absence of fluids influence. In an analogous study in the South Part of the Alpine belt (Grès d'Annot turbidites), we have reported a similar magnetic assemblage [23]. The occurrence of the S3 signal in samples from section B corresponds to the zone where "warm" brines circulated in the Central Appalachians during the Alleghanian Orogeny (e.g., [7]) and ranging from 160 to >200°C in temperature [5,6,8]. Such high temperatures are unlikely to represent the ambient temperatures experienced by the host rocks. Fluid inclusion analyses in Devonian Marcellus Shale [5] show that the sedimentary rocks experienced maximum

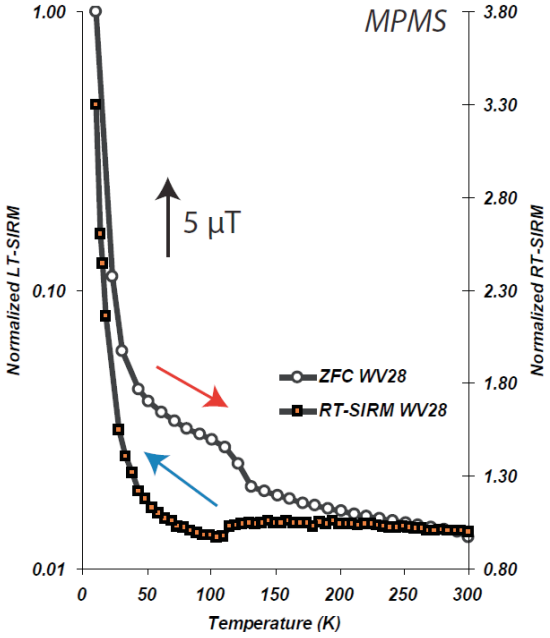

Figure 3. Magnetic signal S3 from the Chemung Group (claystones from section B)

burial temperatures of 120 to 145°C. These "warm" fluids may be also responsible for hydrocarbons flushing from the Valley & Ridge Province into the Appalachian Plateau. Then section B may represent hydrocarbons migration pathway by tectonically driven fluids leading to a reductive environment favoring the formation of magnetite and iron sulfides (e.g., [24]).

At this stage, it remains quite difficult to conclude on the origin of the magnetic assemblages identified in this part of West Virginia.

References

[1] McCabe, C. and Elmore, R.D. (1989), *Rev. Geophys*., 27(4), 471-494.

[2] Lewchuk, M., Evans, M. and Elmore, R.D. (2003), *Geophys. J. Int*., 152, 266-279.

[3] Oliver, J. (1986), *Geology*, 14, 99-102.

[4] Repetski, J., Ryder, R., Lee Avary, K. and Trippi, M. (2005), *Technical Report open-file report* 2005-1078, USGS.

[5] Evans, M. (1995), *Geol. Soc. Am. Bull*., 107(3), 327-339.

[6] Evans, M. (2010), Temporal and spatial changes in deformation conditions during the formation of the Central Appalachian fold-and-thrust belt: evidence from joints, vein mineral paragenesis, and fluid inclusions, In: Tollo, R., Bartholomew, M., Hibbard, J. and Karabinos, P. (eds), From Rodinia to Pangea: the lithotectonic record of the Appalachian Region, *Geological Society of America Memoir*, 206, 477-552.

[7] Evans, M. and Battles, D. (1999), *Geol. Soc. Am. Bull*., 111(12), 1841-1860.

[8] Evans, M. and Elmore, R.D. (2006), *J. Struct. Geol.*, 28, 284-301.

[9] Rochette, P. (1987), *Earth Planet. Sci. Lett*., 84, 446-456.

[10] Crouzet, C., Ménard, G. and Rochette, P. (1999), *Geology*, 27(6), 503-506.

[11] Schill, E., Appel, E. and Gautam, P. (2002), *J. Asian Earth Sci.*, 20, 195-201.

[12] Gillett, S.L. (2003), *J. Geophys. Res.*, 108(B9), 2446.

[13] Rochette, P., Fillion, G. and Dekkers, M.J. (2011), The low-temperature magnetic transition of monoclinic pyrrhotite, *The IRM Quarterly*, 21(1).

[14] Jackson, M. (1990), *J. Geophys. Res*., 95, 2753-2762.

[15] Jackson, M., Sun, W-W. and Craddock, J. (1992), *Geophys. Res. Lett.*, 19(8), 781-784.

[16] Dekkers, M. (1989), *Geophys. J. Int.*, 97, 341-355.

[17] Guyodo, Y., Mostrom, A., Penn, R.L. and Banerjee, S.K. (2003), *Geophys. Res. Lett.*, 30(10), 1512, doi: 10.1029/2003GL017021.

[18] Dekkers, M. (1989), *Phys. Earth Planet. Int.*, 57, 266-283.

[19] Rochette, P., Fillion, G., Mattéi, J-L. and Dekkers, M.J. (1990), *Earth Planet. Sci. Lett*., 98, 319-328.

[20] Aubourg, C. and Pozzi, J-P. (2010), *Earth Planet. Sci. Lett*., 294(1-2), 47-57.

[21] Kars, M., Aubourg, C. and Pozzi, J-P. (2011), *Geophys. J. Int.*, 186, 1029-1035.

[22] Aubourg, C., Pozzi, J-P. and Kars, M. (in press), Burial, claystones remagnetization and some consequences for magnetostratigraphy, in: *Remagnetization and Chemical Alteration of Sedimentary Rocks*, Geological Society of London special volume.

[23] Kars, M., Aubourg, C., Pozzi, J-P., Labaume, P. and Girard, J-P. (2011), Diagenesis to low metamorphism in the Grès d'Annot basin: a magnetic approach, *Geophysical Research Abstracts EGU General Assembly*, 13, EGU2011-5404.

[24] Elmore, R.D., Engel, M.H., Crawford, L., Nick, K., Imbus, S. and Sofer, Z. (1987), *Nature*, 325, 428-430.

Current Articles

A list of current research articles dealing with various topics in the physics and chemistry of magnetism is a regular feature of the IRM Quarterly. Articles published in familiar geology and geophysics journals are included; special emphasis is given to current articles from physics, chemistry, and materials-science journals. Most abstracts are taken from INSPEC (© Institution of Electrical Engineers), Geophysical Abstracts in Press (© American Geophysical Union), and The Earth and Planetary Express (© Elsevier Science Publishers, B.V.), after which they are subjected to Procrustean culling for this newsletter. An extensive reference list of articles (primarily about rock magnetism, the physics and chemistry of magnetism, and some paleomagnetism) is continually updated at the IRM. This list, with more than 10,000 references, is available free of charge. Your contributions both to the list and to the Abstracts section of the IRM Quarterly are always welcome.

Archeomagnetism

Amit, H., M. Korte, J. Aubert, C. Constable, and G. Hulot (2011), The time-dependence of intense archeomagnetic flux patches, *J. Geophys. Res*., 116, B12106, doi:10.1029/2011JB008538.

Carrancho, A., and J. Villalain (2011), Different mechanisms of magnetisation recorded in experimental fires: Archaeomagnetic implications, *Earth Planet. Sci. Lett*., 312, 176-187.

Morales, J., A. Goguitchaichvili, B. Aguilar-Reyes, M. Pineda-Duran, P. Camps, C. Carvallo, and M. Calvo-Rathert (2011), Are ceramics and bricks reliable absolute geomagnetic intensity carriers?, *Phys. Earth Planet. Int.*, 187, 310-321.

Torres, M., V. Costanzo-Alvarez, M. Aldana, N. Suarez, C. Campos, M. M. Mackowiak-Antczak, and M. Brandt (2011), Rock magnetic, petrographic and dielectric characterization of prehistoric Amerindian potsherds from Venezuela, *Stud. Geophys. Geod.*, 55, 717-736.

Bio(geo)magnetism

Gehring, A., H. Fischer, M. Charilaou, and I. Garcia-Rubio (2011), Magnetic anisotropy and Verwey transition of magnetosome chains in Magnetospirillum gryphiswaldense, *Geophys. J. Int*., 187(3), 1215-1221.

Lefevre, C., M. Posfai, F. Abreu, U. Lins, R. Frankel, and D. Bazylinski (2011), Morphological features of elongated-anisotropic magnetosome crystals in magnetotactic bacteria of the Nitrospirae phylum and the Deltaproteobacteria class, *Earth Planet. Sci. Lett*., 312(1-2), 194-200.

Li, B., W. Wu, J. Li, and Y. Pan (2011), Effects of temperature on biomineralization of iron reducing bacteria Shewanella putrefaciens CN32, *Chin. J. Geophys. - CH*, 54(10), 2631-2638.

Nies, D. (2011), How iron is transported into magnetosomes, *Mol. Microbiol*., 82(4), 792-796.

Roberts, A., F. Florindo, G. Villa, L. Chang, L. Jovane, S. Bohaty, J. Larrasoana, D. Heslop, and J. Gerald (2011), Magnetotactic bacterial abundance in pelagic marine environments is limited by organic carbon flux and availability of dissolved iron, *Earth Planet. Sci. Lett.*, 310(3-4), 441-452.

Environmental Magnetism and Paleoclimate Proxies

Balsam, W., B. Ellwood, J. Ji, E. Williams, X. Long, and A. El Hassani (2011), Magnetic susceptibility as a proxy for rainfall: Worldwide data from tropical and temperate climate, *Quat. Sci. Rev.,* 30, 2732-2744.

Duan, Z., X. Gao, Q. Liu, B. Xu, and Y. Su (2011), Magnetic

characteristics of insoluble microparticles in ice core (Nojingkangsang) from the southern Tibetan Plateau and its environmental significance, *Science China – Earth Sci*, 54, 1635-1642.
Font, E., A. Nedelec, B. Ellwood, J. Mirao, and P. Silva (2011), A new sedimentary benchmark for the Deccan Traps volcanism?, *Geophys. Res. Lett*., 38, doi:10.1029/2011GL049824.
Franco, D., L. Hinnov, and M. Ernesto (2012), Millennial-scale climate cycles in Permian-Carboniferous rhythmites: Permanent feature throughout geologic time?, *Geology*, 40(1), 19-22.
Grison, H., E. Petrovsky, N. Jordanova, and A. Kapicka (2011), Strongly magnetic soil developed on a non-magnetic rock basement: A case study from NW Bulgaria, *Stud. Geophys. Geod.*, 55(4), 697-716.
Kardel, F., K. Wuyts, B. Maher, R. Hansard, and R. Samson (2011), Leaf saturation isothermal remanent magnetization (SIRM) as a proxy for particulate matter monitoring: Interspecies differences and in-season variation, *Atmos. Environ*., 45, 5164-5171.
Long, X., J. Ji, and W. Balsam (2011), Rainfall-dependent transformations of iron oxides in a tropical saprolite transect of Hainan Island, South China: Spectral and magnetic measurements, *J. Geophys. Res*., 116, F03015, doi:10.1029/2010JF001712.
Maher, B. (2011), The magnetic properties of Quaternary aeolian dusts and sediments, and their palaeoclimatic significance, *Aeolian Res*., 3(2), 87-144.
Valet, J., E. Moreno, F. Bassinot, L. Johannes, F. Dewilde, T. Bastos, A. Lefort, and M. T. Venec-Peyre (2011), Isolating climatic and paleomagnetic imbricated signals in two marine cores using principal component analysis, *Geochem. Geophys. Geosys*., 12, Q08012, doi:10.1029/2011GC003697.

Extraterrestrial Magnetism

Dwyer, C., D. Stevenson, and F. Nimmo (2011), A long-lived lunar dynamo driven by continuous mechanical stirring, *Nature*, 479(7372), 212-214.
Hoffmann, V., R. Hochleitner, M. Torii, M. Funaki, T. Mikouchi, M. Kaliwoda, P. Jenniskens, and M. Shaddad (2011), Magnetism and mineralogy of Almahata Sitta polymict ureilite (= asteroid 2008 TC3): Implications for the ureilite parent body magnetic field, *Meteorit. Planet. Sci*., 46(10), 1551-1564.
Le Bars, M., M. Wieczorek, O. Karatekin, D. Cebron, and M. Laneuville (2011), An impact-driven dynamo for the early Moon, *Nature*, 479(7372), 215-U90.
Ravat, D. (2011), Interpretation of Mars southern highlands high amplitude magnetic field with total gradient and fractal source modeling: New insights into the magnetic mystery of Mars, *Icarus*, 214(2), 400-412.
Yu, Y., S. Doh, W. Kim, and K. Min (2011), Origin of stable remanent magnetization in LL6 chondrite, St. Severin, *Phys. Earth Planet. Int.*, 187(3-4), 292-300.

Geomagnetism and Geodynamo Studies

Aubert, J., and A. Fournier (2011), Inferring internal properties of Earth's core dynamics and their evolution from surface observations and a numerical geodynamo model, *Nonlinear Processes Geophys*., 18(5), 657-674.
Bazhenov, M., N. Levashova (2011), Directional secular variation of the geomagnetic field in Late Devonian volcanics of the Northern Tien Shan, *Izv. Phys. Solid Earth*, 47, 1094-1105.
Christensen, U. (2011), Geodynamo models: Tools for understanding properties of Earth's magnetic field, *Phys. Earth Planet. Int*., 187(3-4), 157-169.
Constable, C. (2011), Modelling the geomagnetic field from syntheses of paleomagnetic data, *Phys. Earth Planet. Int*., 187, 109-117.
Korte, M., and C. Constable (2011), Improving geomagnetic field reconstructions for 0-3 ka, *Phys. Earth Planet. Int*., 188, 247-259.
Laj, C., C. Kissel, C. Davies, and D. Gubbins (2011), Geomagnetic field intensity and inclination records from Hawaii and the Reunion Island: Geomagnetic implications, *Phys. Earth Planet. Int*., 187, 170-187.
Li, K., A. Jackson, and P. Livermore (2011), Variational data assimilation for the initial-value dynamo problem, *Phys. Rev. E*, 84, 056321.
Linder, J., and S. Gilder (2011), Geomagnetic secular variation recorded by sediments deposited during the Cretaceous normal superchron at low latitude, *Phys. Earth Planet. Int.*, 187(3-4), 245-260.
Pinheiro, K., A. Jackson, C. Finlay (2011), Measurements and uncertainties of the occurrence time of the 1969, 1978, 1991, and 1999 geomagnetic jerks, Geochem. Geophys. Geosys., 12, Q10015, doi:10.1029/2011GC003706.
Smirnov, A., J. Tarduno, and D. Evans (2011), Evolving core conditions ca. 2 billion years ago detected by paleosecular variation, *Phys. Earth Planet. Int.*, 187(3-4), 225-231.
Smith-Boughner, L. T., L. Ziegler, and C. Constable (2011), Changing spectrum of geomagnetic intensity variations in a fragmented 12 My sediment record from the Oligocene, *Phys. Earth Planet. Int*., 188(3-4), 260-269.
St-Onge, G., and J. Stoner (2011), Paleomagnetism near the north magnetic pole: A Unique Vantage Point for Understanding the Dynamics of the Geomagnetic Field and Its Secular Variations, *Oceanography*, 24(3), 42-50.

Magnetic Field Records and Paleointensity Methods

Calvo-Rathert, M., A. Goguitchaichvili, M. Bogalo, N. Vegas-Tubia, A. Carrancho, and J. Sologashvili (2011), A paleomagnetic and paleointensity study on Pleistocene and Pliocene basaltic flows from the Djavakheti Highland (Southern Georgia, Caucasus), *Phys. Earth Planet. Int*., 187(3-4), 212-224.
Camps, P., B. Singer, C. Carvallo, A. Goguitchaichvili, G. Fanjat, and B. Allen (2011), The Kamikatsura event and the Matuyama-Brunhes reversal recorded in lavas from Tjornes Peninsula, northern Iceland, *Earth Planet. Sci. Let*t., 310, 33-44.
Donadini, F., S. Elming, L. Tauxe, and U. Halenius (2011), Paleointensity determination on a 1.786 Ga old gabbro from Hoting, Central Sweden, *Earth Planet. Sci. Lett*., 309, 234-248.
Dunlop, D. (2011), Physical basis of the Thellier-Thellier and related paleointensity methods, *Phys. Earth Planet. Int*., 187, 118-138.
Jicha, B., L. Kristjansson, M. Brown, B. Singer, B. Beard, and C. Johnson (2011), New age for the Skalamaelifell excursion and identification of a global geomagnetic event in the late Brunhes chron, *Earth Planet. Sci. Lett*., 310(3-4), 509-517.
Kissel, C., H. Guillou, C. Laj, J. Carracedo, S. Nomade, F. Perez-Torrado, and C. Wandres (2011), The Mono Lake excursion recorded in phonolitic lavas from Tenerife (Canary Islands): Paleomagnetic analyses and coupled K/Ar and Ar/Ar dating, *Phys. Earth Planet. Int.*, 187(3-4), 232-244.
Kurazhkovskii, A., N. Kurazhkovskaya, and B. Klain (2011), Calibration of geomagnetic paleointensity data based on redeposition of sedimentary rocks, *Phys. Earth Planet. Int*., 189, 109-116.
Lascu, I., and J. Feinberg (2011), Speleothem magnetism, *Quat. Sci. Rev*., 30, 3306-3320.
Muxworthy, A., X. Ji, V. Ridley, Y. Pan, L. Chang, L. Wang, and A. Roberts (2011), Multi-protocol palaeointensity determination from middle Brunhes Chron volcanics, Datong Volcanic

Province, China, *Phys. Earth Planet. Int.*, 187(3-4), 188-198.
Nilsson, A., R. Muscheler, I. Snowball, A. Aldahan, G. Possnert, P. Augustinus, D. Atkin, and T. Stephens (2011), Multi-proxy identification of the Laschamp geomagnetic field excursion in Lake Pupuke, New Zealand, *Earth Planet. Sci. Lett.*, 311, 155-164.
Paterson, G. (2011), A simple test for the presence of multidomain behavior during paleointensity experiments, *J. Geophys. Res.*, 116, doi:10.1029/2011JB008369.
Qin, H., H. He, Q. Liu, and S. Cai (2011), Palaeointensity just at the onset of the Cretaceous normal superchron, *Phys. Earth Planet. Int*., 187(3-4), 199-211.
Sagnotti, L., P. Macri, R. Lucchi, M. Rebesco, and A. Camerlenghi (2011), A Holocene paleosecular variation record from the northwestern Barents Sea continental margin, *Geochem. Geophys. Geosys*., 12, Q11Z33, doi:10.1029/2011GC003810.
Shaar, R., N. Ron, L. Tauxe, R. Kessel, and A. Agnon (2011), Paleomagnetic field intensity derived from non-SD: Testing the Thellier IZZI technique on MD slag and a new bootstrap procedure, *Earth Planet. Sci. Lett*., 310(3-4), 213-224.
Shcherbakova, V., D. Kovalenko, V. Shcherbakov, and G. Zhidkov (2011), Paleointensity of the geomagnetic field in the Cretaceous (from Cretaceous rocks of Mongolia), *Izv. Phys. Solid Earth*, 47(9), 775-791.
Stanton, T., A. Nilsson, I. Snowball, and R. Muscheler (2011), Assessing the reliability of Holocene relative palaeointensity estimates: a case study from Swedish varved lake sediments, *Geophys. J. In*t., 187(3), 1195-1214.

Magnetic Remanence and Remanence Acquisition Processes

Jin, C., and Q. Liu (2011), Remagnetization mechanism and a new age model for L9 in Chinese loess, *Phys. Earth Planet. Int*., 187(3-4), 261-275.
Liu, C., K. Ge, C. Zhang, Q. Liu, C. Deng, and R. Zhu (2011), Nature of remagnetization of Lower Triassic red beds in southwestern China, *Geophys. J. Int*., 187(3), 1237-1249.
Løvlie, R., R. Wang, and X. Wang (2011), In situ remagnetization experiments of loess on the Chinese Loess Plateau: Evidence for localized post-depositional remanent magnetization, *Geochem. Geophys. Geosys*., 12, Q12015, doi:10.1029/2011GC003830.
Suganuma, Y., J. Okuno, D. Heslop, A. Roberts, T. Yamazaki, and Y. Yokoyama (2011), Post-depositional remanent magnetization lock-in for marine sediments deduced from ^{10}Be and paleomagnetic records through the Matuyama-Brunhes boundary, *Earth Planet. Sci. Lett*., 311, 39-52.
Yu, Y. (2011), Importance of cooling rate dependence of thermoremanence in paleointensity determination, *J. Geophys. Res*., 116, B09101, doi:10.1029/2011JB008388.

Rock and Mineral Magnetism

Brownlee, S., J. Feinberg, T. Kasama, R. Harrison, G. Scott, and P. Renne (2011), Magnetic properties of ilmenite-hematite single crystals from the Ecstall pluton near Prince Rupert, British Columbia, *Geochem. Geophys. Geosys*., 12, Q07Z29, doi:10.1029/2011GC003622.
Cicchino, A., E. Zanella, G. De Astis, R. Lanza, F. Lucchi, C. Tranne, G. Airoldi, and S. Mana (2011), Rock magnetism and compositional investigation of Brown Tuffs deposits at Lipari and Vulcano (Aeolian Islands - Italy), *J. Volcanol. Geotherm. Res*., 208, 23-38.
Gilder, S., R. Egli, R. Hochleitner, S. Roud, M. Volk, M. Le Goff, M. De Wit (2011), Anatomy of a pressure-induced, ferromagnetic-to-paramagnetic transition in pyrrhotite: Implications for the formation pressure of diamonds, *J. Geophys. Res*., 116.
Jovane, L., E. Yokoyama, T. Seda, R. Burmester, R. Trindade, and B. Housen (2011), Rock magnetism of hematitic "bombs" from the Araguainha impact structure, Brazil, *Geochem. Geophys. Geosys*., 12, Q12Z34, doi:10.1029/2011GC003758.
Lappe, S., N. Church, T. Kasama, A. Fanta, G. Bromiley, R. E. Dunin-Borkowski, J. Feinberg, S. Russell, and R. Harrison (2011), Mineral magnetism of dusty olivine: A credible recorder of pre-accretionary remanence, *Geochem. Geophys. Geosys*., 12, Q12Z35, doi:10.1029/2011GC003811.
Mitra, R., L. Tauxe, and J. Gee (2011), Detecting uniaxial single domain grains with a modified IRM technique, *Geophys. J. Int*., 187(3), 1250-1258.
Raiskila, S., J. Salminen, T. Elbra, and L. Pesonen (2011), Rock magnetic and paleomagnetic study of the Keurusselka impact structure, central Finland, *Meteorit. Planet. Sci*., 46, 1670-1687.

Mineral Physics and Chemistry

Senn, M., J. Wright, and J. Attfield (2012), Charge order and three-site distortions in the Verwey structure of magnetite, *Nature*, 481(7380), 173-176.
Wenk, H., K. Chen, and R. Smith (2011), Morphology and microstructure of magnetite and ilmenite inclusions in plagioclase from Adirondack anorthositic gneiss, *Am. Mineral*., 96, 1316-1324.
Williams, W., A. Muxworthy, and M. Evans (2011), A micromagnetic investigation of magnetite grains in the form of Platonic polyhedra with surface roughness, *Geochem. Geophys. Geosys.*, 12, Q10Z31, doi:10.1029/2011GC003560.
Zinin, P., L. Tatsumi-Petrochilos, L. Bonal, T. Acosta, J. Hammer, S. Gilder, and M. Fuller (2011), Raman spectroscopy of titanomagnetites: Calibration of the intensity of Raman peaks as a sensitive indicator for their Ti content, *Am. Mineral*., 96, 1537-1546.

Tectonics/Paleomagnetism

Domeier, M., R. Van Der Voo, and F. Denny (2011), Widespread inclination shallowing in Permian and Triassic paleomagnetic data from Laurentia: Support from new paleomagnetic data from Middle Permian shallow intrusions in southern Illinois (USA) and virtual geomagnetic pole distributions, *Tectonophys*., 511(1-2), 38-52.
Eriksson, P., M. Rigby, P. Bandopadhyay, and N. Steenkamp (2011), The Kaapvaal Craton, South Africa: no evidence for a supercontinental affinity prior to 2.0 Ga?, *Int. Geol. Rev.*, 53, 1312-1330.
Granot, R., M. Abelson, H. Ron, M. Lusk, and A. Agnon (2011), Direct evidence for dynamic magma supply fossilized in the lower oceanic crust of the Troodos ophiolite, *Geophys. Res. Lett.*, 38, L16311, doi:10.1029/2011GL048220.
Horst, A., R. Varga, J. Gee, and J. Karson (2011), Paleomagnetic constraints on deformation of superfast-spread oceanic crust exposed at Pito Deep Rift, *J. Geophys. Res*., 116, doi:10.1029/2011JB008268.
Hyodo, M., S. Matsu'Ura, Y. Kamishima, M. Kondo, Y. Takeshita, I. Kitaba, T. Danhara, F. Aziz, I. Kurniawan, and H. Kumai (2011), High-resolution record of the Matuyama-Brunhes transition constrains the age of Javanese Homo erectus in the Sangiran dome, Indonesia, *PNAS*, 108(49), 19563-19568.

Other

Usui, Y., M. Uehara, and K. Okuno (2012), A rapid inversion and resolution analysis of magnetic microscope data by the subtractive optimally localized averages method, *Comput. Geosci*., 38, 145-155.

energy is >> cubic magnetocrystalline energy, it plays a dominant role in controlling magnetization at $T < T_v$.

Pioneering Studies

The application of a magnetic field applied during cooling through the Verwey transition can have strong effects on the physical properties of the low-temperature Fe_3O_4 polymorph, as first reported by Li (1932). Working with natural single-crystal magnetite samples cut into disks parallel to the (100), (110) and (111) planes, Li measured components of in-plane magnetization parallel and perpendicular (M_{perp}) to an applied field, at temperatures just above and just below T_v (Fig. 2). His Figures 11 and 13, reproduced here (Fig. 3), show M_{perp} as a function of applied field angle in the (111) plane, for the two temperatures. Above T_v there are three maxima and three minima over the 180-degree range of orientations, showing the triaxial anisotropy expected for a cubic crystal in that plane. Below T_v, in contrast, a strong uniaxial anisotropy is indicated by the high-amplitude M_{perp} curve with a single maximum and minimum.

When Li changed the orientation of the field applied during cooling through T_v, he discovered that the anisotropy of the low-T magnetite changed accordingly (Fig. 4), leading him to write "It seems as if we can locate the position of maxima and minima of the curves of these two components in any position that we please, depending on the position of the field when it is cooling." We are accustomed to thinking of a crystal with fixed easy-axis orientations along which the magnetic moment aligns itself to minimize energy; here we have the reciprocal situation, in which the easy axis aligns itself with a moment whose orientation is fixed by a strong applied field. Li also found that cooling through T_v without an applied field yielded a weak triaxial anisotropy. This was the first of what have come to be known as "FC-ZFC" experiments, involving comparison of low-temperature properties in the field-cooled (FC) and zero-field-cooled (ZFC) states.

Verwey was inspired by Li's results to perform his own FC-ZFC experiment. His model of charge ordering in the low-T state of magnetite involved ferrous and ferric ions occurring in alternating (001) planes and aligned along [110] or [-110]. This suggested that conductivity should be anisotropic, but "this will be measurable only if the direction of the tetragonal axis can be fixed. Ching Hsien Li has found that a single crystal of Fe_30_4 becomes magnetically anisotropic at low temperature. Hence it seems possible to fix the tetragonal axis with the aid of a magnetic field." Lacking good single crystals upon which to experiment, Verwey et al. (1947) "had to use, therefore, sintered bars of pure Fe_30_4, consisting of agglomerates of small crystals oriented in all directions, where the expected effect will be reduced considerably." Nevertheless they found a significant FC-ZFC-related anisotropy, with conductivities (in units of 10^{-3} ohm^{-1} cm^{-1}) of 7.19 parallel to the cooling field, 6.18 perpendicular to it, and 6.45 for the ZFC case. This supported the charge ordering model, with conductivity "highest in directions where Fe^{2+} and Fe^{3+} alternate, and lowest in directions where one meets either only Fe^{2+} or only Fe^{3+} ions. Hence it is to be expected that the conductivity will be highest parallel to the magnetic field; that is, more or less parallel to the directions in which the c-axis has been 'frozen in.'"

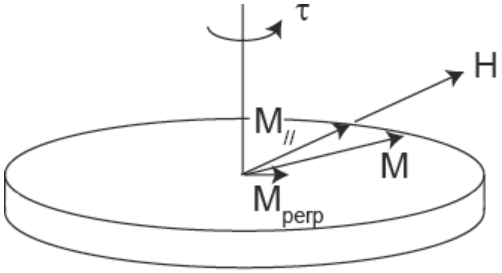

Figure 2. Schematic demonstrating torque experiments of Li (1932) described above.

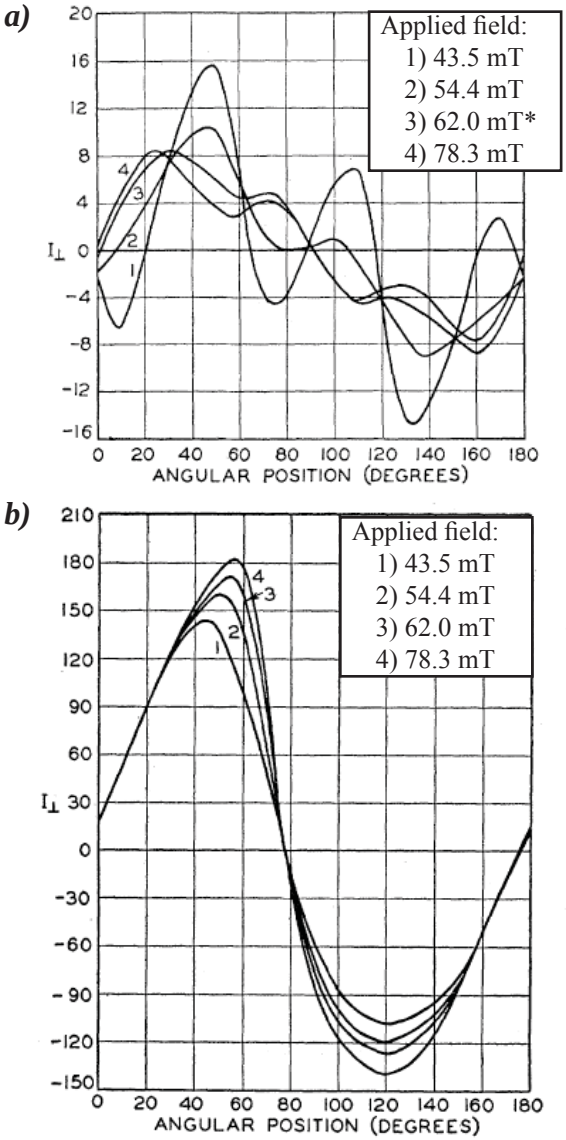

*Figure 3. The normal component of in-plane (111) magnetization at 118 K (a) and at 107 K (b), plotted against angular position. From Li (1932; Figs. 11, 12). *The original caption reads 43.5 mT, but we assume this is a typo.*

After various x-ray studies had failed to provide a clear picture of the crystallography of the low-T phase, Bickford (1953) directly measured changes in length along different crystal orientations during cooling or warming through the transition, using strain gauges cemented to

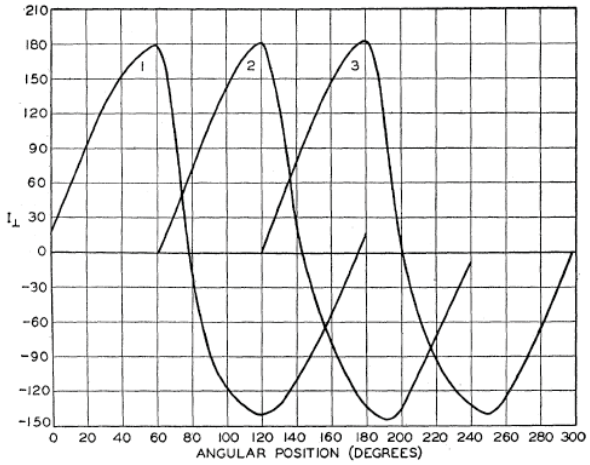

Figure 4. The normal component of in-plane (111) magnetization following cooling through 113 K with the field aligned with the marked 0 direction on the crystal (1), with the field aligned 60° from the 0 direction (2), and with the field alinged 120° from the 0 position (3). From Li (1932, Fig. 16).

single-crystal specimens. The cubic <100> most closely aligned with a cooling field was found to shorten by a small amount on becoming the monoclinic c axis, whereas the two perpendicular cube edges expanded slightly. Accordingly, Bickford found that c-axis selection could also be accomplished by applying uniaxial pressure along one of the cube edges during cooling, although somewhat less effectively than by field cooling, as evidenced by low-T hysteresis measurements (Fig. 5). He also discovered that the c-axis established by field cooling could still be changed at 98 K by applying a strong field along one of the other cube edge orientations. Maximum extension on cooling through T_v occurred along the cubic <110> that becomes the monoclinic a-axis. Bickford suggested that a twin-free monoclinic crystal could be produced by a combination of FC c-axis selection and compression along one of the <110> axes perpendicular to the cooling field, to control the a-axis orientation. A similar scheme was later used by Abe et al (1976) to produce untwinned single crystals for low-T torque measurements to determine the monoclinic anisotropy constants.

Effects on Remanence Acquired at $T < T_v$

Remanence acquired in the low temperature state depends on whether or not the sample was cooled in a field through Tv, and there are some counterintuitive differences between the single-domain (SD) and multi-domain (MD) cases. When this low-T remanence is heated through T_v, remanence is lost as the magnetocrystalline anisotropy changes by a factor of about fifteen, and the easy axis of magnetization typically changes due to the shifting balance between crystallographic and shape control. In MD particles various additional factors contribute to changes in remanence, and in general the effects of the Verwey transition are more pronounced in larger particles. We start by describing the (relatively) simple SD case.

Single Domain Case

Imagine a population of SD magnetite with randomly-oriented crystallographic axes, magnetized to saturation, and cooling through T_v in a 2.5-T applied field. To minimize energy, the monoclinic c axis forms in each particle along the cube edge closest to the applied field, and when the field is removed after further cooling, the moment of each particle rotates from the applied field direction into alignment with this easy axis. Think about it for a moment and you will see that the remanence acquired by such a population through the FC process is exactly the same as that which would be acquired by isothermal magnetization of randomly-oriented SD particles having cubic anisotropy and easy axes along <100>, i.e., $0.832*M_s$ (e.g., Dunlop & Özdemir, 1997, eq 11.16). In contrast, random c-axis selection during ZFC yields an isotropic population of monoclinic grains which, when magnetized isothermally in a strong field, acquires a low-T SIRM equal to $0.5*M_s$ (the same as the room-T SIRM acquired by a population of uniaxial SD particles). The ratio of intensities M_{FC}/M_{ZFC} for these ideal SD populations at low temperature is therefore 0.832/0.5=1.664. This ratio has been labelled R_{LT} by Smirnov (2009), who measured it as a function of grain size for magnetites of variable stoichiometry, finding maximum values near 1.3 for his finest-grained samples. Similar results are shown in Figure 7 for silicate grains with magnetite inclusions from the Bushveld complex (J. Feinberg, unpublished data).

We noted above that for particles cooled in the absence of a field, c-axis selection is commonly considered to be a random process. Alternatively, however, it has been suggested (Bickford, 1953; Medrano et al., 1999; Smirnov and Tarduno, 2002; Muxworthy and Williams, 2006; Kasama et al 2010), that ZFC c-axis selection may be influenced or controlled by magnetic moment orientations during cooling through T_v, although to a much lesser degree than for FC. In this case, a c-axis is selected which is closest to the high-temperature ($T>T_v$) moment of each individual grain or domain.

Having produced low-T FC and ZFC remanent

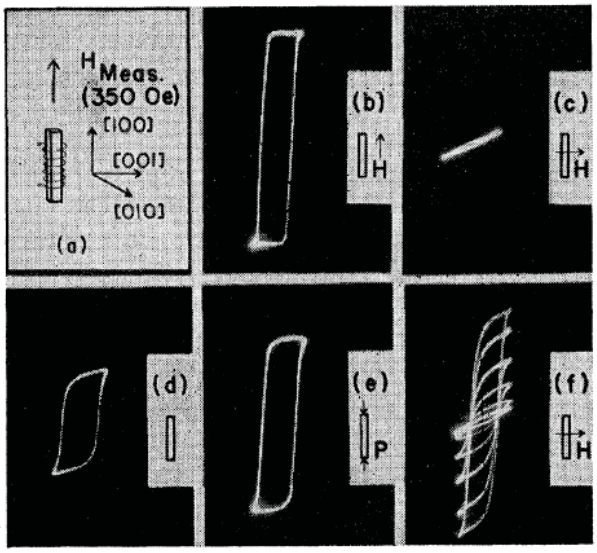

Figure 5. Hysteresis loops at 88 K for a single magnetite crystal. a) Schematic showing direction of measurement field with respect to crystal. b) Loop after cooling through T_v with field parallel to measurement axis. c) After cooling with field perpendicular to measurement axis. d) After cooling in zero field. e) After cooling in zero field, but with pressure applied along measurement axis. f) Cooling as in (c), but loops measured on warming through T_v. From Bickford (1953; Fig. 2)

magnetizations, let us now consider what happens while warming them through T_v. A decrease in net magnetization results as individual SD particle moments rotate from one easy axis at low temperature to another at high temperature (Fig. 6). Two things that we might expect based on common-sense reasoning turn out to be generally true. First, the intensity of remanence remaining above T_v is the same for both the FC and ZFC cases (since the FC-induced anisotropy disappears, and the distribution of easy-axis orientations is the same as in the ZFC case). Second, the magnitude of the remanence loss is related to the relative magnitude of the shape and magnetocrystalline anisotropy energies. Although at $T < T_v$ magnetocrystalline anisotropy is dominant, shape is still important and the remanent moment of each SD particle orients itself somewhere between the crystallographic c-axis and the dimensional long axis. Particles with higher aspect rations will therefore suffer less remanence loss on warming. Numerical models (Carter-Stiglitz et al., 2002) showed that for randomly-oriented particles with weak shape anisotropy, a ZFC low-T SIRM loses half its remanence on warming through T_v, and the fractional loss diminishes with increasing elongation, as well as with increasing grain

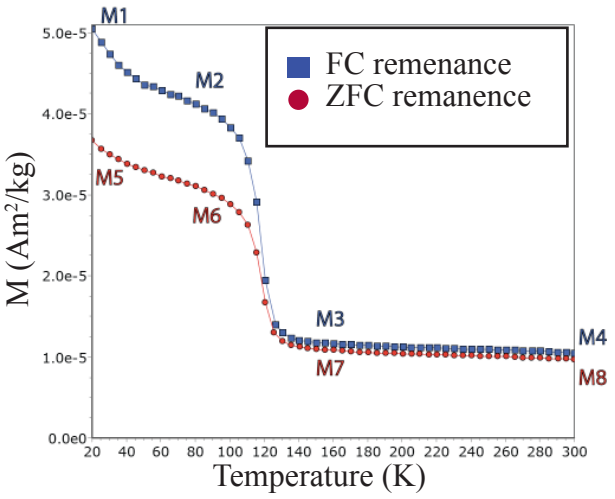

Figure 6. Anatomy of an FC-ZFC remanence data set. Squares show zero-field warming (M1 through M4) of a remanence acquired by field-cooling from 300K in a 2.5-T field; circles show zero-field warming (M5 through M8) of a remanence acquired isothermally in a 2.5-T at 20 K after zero-field-cooling from 300K. In both cases the loss of remanence associated with the monoclinic-to-cubic transition occurs over a range of temperatures around Tv, from about 100K to 130K for this sample (a plagioclase crystal from the Bushveld Complex containing exsolved SD magnetite; unpublished data of J. M. Feinberg).

Quantities calculated form such data sets typically include estimates of Tv and of the associated loss of remanence. The transition temperature is most commonly quantified as the point of maximum (negative) slope, about 118 K here. Alternatively it can be taken to coincide with the point of maximum upward curvature at a slightly higher temperature (123.5K in this data set), analogous to the "two-tangents" method of defining Curie temperatures from strong-field thermomagnetic data. The remanence drop can be quantified in several ways. Moskowitz et al. (1993) defined the "delta" parameters δ_{FC} = (M2-M3)/M2 and δ_{ZFC} = (M6-M7)/M6 as the fractional remanence loss between 80K and 150K. The ratio δ_{FC}/δ_{ZFC} is in general an indicator of magnetite grain size (values greater than one occurring only for SD populations, and values ~1 for all larger sizes). Smirnov (2009) defines the R_{LT} ratio (=M1/M5) and shows that it covers a wider range of values, less than 1 for MD populations (down to about 0.6) and greater than 1 for SD samples (up to about 1.3).

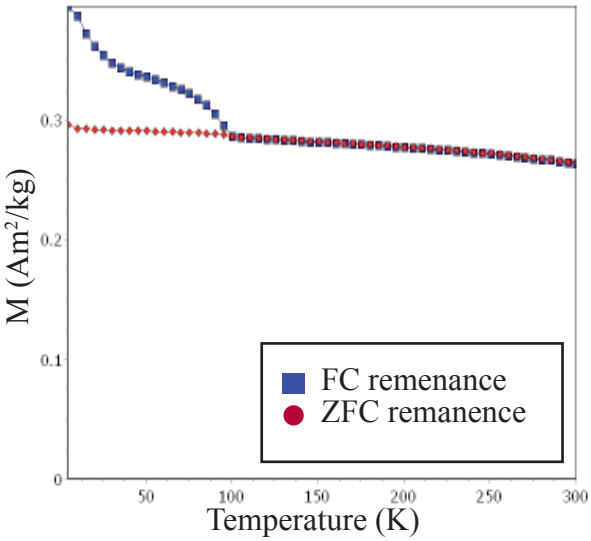

Figure 7. Sample with intact bacterial magnetosome chains, somewhat oxidized by exposure to air (Tv ~100K).

size (also seen in experimental data, Özdemir et al., 2002).

Moskowitz et al. (1993) observed that variation in magnetization across T_v serves as a diagnostic indicator of magnetosomes in intact chains. For a magnetization acquired at low temperature the fractional loss of remanence on warming across T_v is defined as $\partial = (M^{80K}-M^{150K})/M^{80K}$. Moskowitz et al. (1993) observed that the loss for a remanence acquired after cooling in a strong field (∂_{FC}) is always greater than that for a ZFC remanence (∂_{ZFC}). This, as described above, is expected for all SD populations, biogenic or not, due to the induced anisotropy of the FC state. But notably, Moskowitz et al. (1993) found that the ∂-ratio ($\partial_{FC}/\partial_{ZFC}$) was > 2 for intact magnetosome chains and < 2 for samples with inorganic SD particles or with disrupted chains. It is easy to imagine factors that may be responsible for this unique signature of bacterial magnetosome chains. Often the magnetosomes have shape and room-temperature crystallographic easy axes that coincide: they are "manufactured" to be elongated along a <111> axis. Moreover there are strong magnetostatic interactions among neighboring particles in the intracellular chains.

These factors were simulated in numerical models by Carter-Stiglitz et al. (2004), who found that elevated ∂-ratios can best be explained by non-stoichiometry. We will cover this topic extensively in a future article; for the present we will simply note that maghemitization results in a decrease in magnetocrystalline anisotropy at $T < T_v$, thus resulting in a decreasing ∂ in both FC and ZFC curves. As can be seen in Figure 7, ∂_{ZFC} is often very low in samples with bacterial magnetite, and consequently the ∂-ratio can be quite large (up to about 6 in the models of Carter-Stiglitz et al., 2004). The effects of partial maghemitization are greater in the ZFC case, because in the FC case there is an easy-axis bias. Thus, the elevated ∂-ratios are a sensitive indicator of SSD magnetite, but not conclusively biogenic in origin. Furthermore, the experimental and modeling results suggest that magnetosomes become partially oxidized extremely rapidly and/or they may not produce perfectly stoichiometric magnetite.

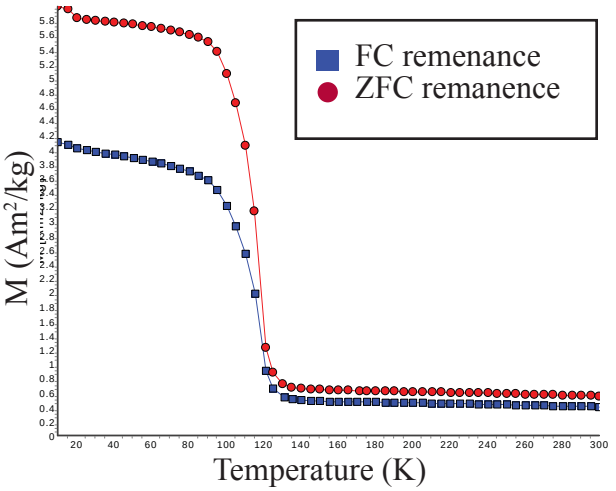

Figure 8. Wright magnetite 041183 (nominal size = 14 μm). Note that a characteristic feature of MD magnetite is a ZFC remenance that is larger than an FC remenance. Also note a greater loss of remanence on warming across T_v compared to the SD case (Fig. 7).

Multi-Domain Case

When MD magnetite cools through T_v, the resulting magnetic state is complicated (compared to the SD case) by the presence of both domain walls and transformational twins. Kasama et al. (2010) indicate 24 possible orientational variants, each having the monoclinic c-axis aligned along one of the cubic <100> axes and the monoclinic a-axis along one of the cubic face diagonals perpendicular to c. Twin domains with any of these orientations are separated by twin walls from other twin domains having differing orientations. Various configurations are possible; for example a twin wall may separate domains having different hard (a) axis orientations but identical easy axes, or the wall may be a boundary where two c-axes intersect at right angles. Because of the intense magnetocrystalline anisotropy, the latter type of twin wall is also necessarily a 90° domain wall. Such twin configurations and the resultant immobile domain walls exert strong controls on the low-T magnetitc properties of magnetite. Kasama et al. (2010) have produced amazing videos of the monoclinic twins nucleating and growing in cubic magnetite as it cools through T_v.

One of the peculiar features of MD magnetite is that in contrast to the SD case, a ZFC low-T SIRM has a higher intensity than a FC SIRM (Fig. 8). This was first reported by Brachfeld et al. (2001, 2002) and was also observed by Kosterov (2001, 2003) who proposed that the degree of easy-axis alignment with respect to the applied field (at low-T) could lead to lowered coercivity in the FC state. Further work (Carter-Stiglitz et al., 2006; Kosterov & Fabian 2008) suggests that the elevated remanence in the ZFC state arises from the twin boundaries which serve to pin domain walls and produce an effectively smaller magnetic grain size. In the FC case, the formation of twins is suppressed (particularly those with c axes at a high angle to the cooling field) because of the field-induced easy axis selection (described above), resulting in an overall softer magnetization. The 180° domain walls that form in this case are more easily moved than the 90° twin boundaries/domain walls that form in the ZFC case.

Susceptibility and hysteresis in the FC and ZFC states

Space limitations and basic human decency prevent us from plunging into all the gory details, but for MD magnetite, the hard wall pinning in the twinned low-T state that is responsible for retention of strong ZFC remanence can also be seen in low-field susceptibility and high-field hysteresis measurements as functions of temperature and cooling fields (Kosterov 2003; Carter-Stiglitz et al. 2006; Kosterov & Fabian 2008). The monoclinic phase is significantly harder magnetically in the ZFC state than in the FC state (when measurements are made parallel to the cooling field), having lower susceptibility (Fig. 9), higher coercivity, and higher M_r/M_s ratios.

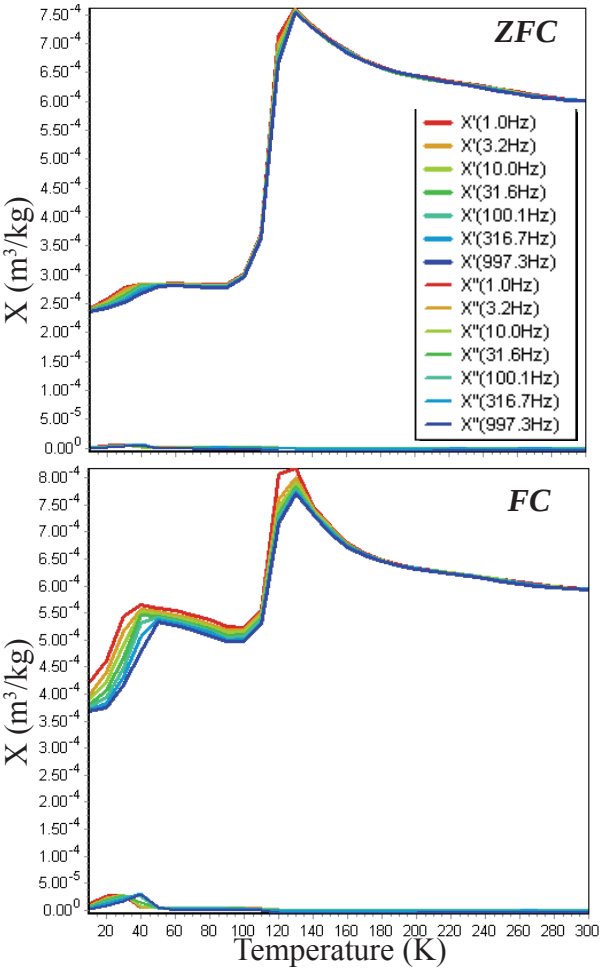

Figure 9. Wright magnetite 041183 (nominal size = 14 μm). Susceptibility (measured in 7 frequencies from 1-100 Hz) measured on warming following zero-field cooling (top) and field cooling (bottom). Note that the origin of the anomaly ~ 50K is unknown and will be the subject of a future article.

Pseudo-Single-Domain Case

Many properties of PSD grains are indistinguishable from those of suitable mixtures of SD and MD grains (e.g., Dunlop, 2002), and to a large extent the same is also true of simple FC-ZFC remanence experiments. For example, an observed R_{LT} approximately equal to one could correspond to a mixture of SD (R_{LT} >1) and MD (R_{LT} <1) particles, or it could be due to a unimodal distribution of intermediate-sized PSD grains. However Smirnov (2006a,b, 2007) has discovered some distinctive PSD behavior at low temperatures in hysteresis and FORC measurements in

the FC and ZFC states. In the "field memory effect", low-T hysteresis loops exhibit some distortion in the field range corresponding to the cooling field (several mT to tens of mT) and FORC diagrams exhibit double peaks, roughly symmetric around a horizontal line corresponding to the cooling field. These effects were found only in unimodal populations with sizes in the PSD range; SD and MD populations and mixtures thereof exhibited no "field memory" effects.

Behavior of other minerals in FC-ZFC experiments

Quantitative measures of Verwey-transition-related behavior generally get fouled up by the presence of other remanence-carrying phases in natural samples. Maghemite and greigite have no low-temperature transitions, and when they are thermally stable (larger than the SP-SSD threshold at room temperature) their remanence is almost independent of temperature for T < 300K. A large contribution from either therefore drives R_{LT} towards 1, and ∂_{FC} and ∂_{ZFC} towards zero; the ratio $\partial_{FC}/\partial_{ZFC}$ nevertheless remains a good indicator of the presence of bacterial magnetite as long as at least 10% of the remanence is carried by intact magnetosome chains (Moskowitz et al., 1993). Things are more troublesome when there are significant contributions from other magnetites (e.g., collapsed chains or detrital populations); in such situations the "bug test" gives a positive result only when 80-90% or more of the remanence is due to magnetosome chains.

Goethite is another villain in the bacterial magnetite story. It has no low-temperature transition, but there is usually a very large difference between FC and ZFC remanences due to the combination of very high coercivity and relatively low ordering temperature (~400K; Özdemir and Dunlop, 1996). Isothermal strong-field magnetization at 10K or 20K is quite ineffective at producing a strong remanence in the ZFC state in this very hard material, even when 2.5 T is applied; cooling in the same field from 300K (T/T_N~0.75) magnetizes much more efficiently through the combined thermal and magnetic field energies, in effect producing a strong-field pTRM. R_{LT} is commonly 5 or more, and ∂_{FC} can sometimes be larger for pure goethite than for pure bacterial magnetites.

References

Abe, K., Y. Miyamoto, and S. Chikazumi (1976), Magnetocrystalline anisotropy of low temperature phase of magnetite, *J. Phys. Soc. Japan*, 41,1894-1902.

Bickford, L. R., Jr. (1953), The low temperature transformation in ferrites, *Rev. Mod. Phys*., 25, 75–79

Brachfeld, S., Y. Guyodo, and G.D. Acton (2001), Data report: The magnetic mineral assemblage of hemiplagic drifts, ODP Site 1096, In Barker, P.F., Camerlenghi, A., Acton,G.D., and Ramsay, A.T.S. (Eds.), *Proc. ODP, Sci. Results*, 178, 1–12

Brachfeld, S.A., S.K. Banerjee, Y. Guyodo, G.D. Acton (2002), A 13200 year history of century to millennial-scale paleoenvironmental change magnetically recorded in the Palmer Deep, western Antarctic Peninsula, *Earth Planet. Sci. Lett*., 194, 311-326.

Carter-Stiglitz, B., M. Jackson, and B. Moskowitz (2002), Low-temperature remanence in stable single domain magnetite, *Geophys. Res. Lett.*, 29. (See also correction v.30, n.21, 2113, 2003)

Carter-Stiglitz, B., B. Moskowitz, and M. Jackson (2004), More on the low-temperature magnetism of stable single domain magnetite: Reversibility and non-stoichiometry, *Geophys. Res. Lett*., 31, L06606, doi:10.1029/2003GL019155.

Carter-Stiglitz, B., B. Moskowitz, P. Solheid, T.S. Berquó, M. Jackson, and A. Kosterov (2006), Low-temperature magnetic behavior of multidomain titanomagnetites: TM0, TM16, and TM35, *J. Geophys. Res*., 111, B12S05, doi:10.1029/2006JB004561.

Dunlop, D.J., and Ö. Özdemir (1997), *Rock Magnetism: Fundamentals and frontiers*, Cambridge University Press, New York, 573pp.

Dunlop, D.J. (2002), Theory and application of the Day plot (M_{rs}/M_s versus H_{cr}/H_c) 1. Theoretical curves and tests using titanomagnetite data, *J. Geophys. Res.*, 107, doi: doi:10.1029/2006JB004561.

Kasama, T., N.S. Church, J.M. Feinberg, R.E. Dunin-Borkowski, and R.J. Harrison (2010), Direct observation of ferrimagnetic/ferroelastic domain interactions in magnetite below the Verwey transition, *Earth Planet. Sci. Lett*., 297, 10-17.

Kosterov, A. (2001), Magnetic hysteresis of pseudo-single-domain and multidomain magnetite below the Verwey transition, *Earth Planet. Sci. Lett*., 186, 245-253.

Kosterov, A., (2003), Low-temperature magnetization and AC susceptibility of magnetite: effect of thermomagnetic history, *Geophys. J. Int*., 154, 58-71.

Kosterov, A., and K. Fabian (2008), Twinning control of magnetic properties of multidomain magnetite below the Verwey transition revealed by measurements on individual particles, *Geophys. J. Int.*, 174(1), 93-106

Li, C. H. (1932), Magnetic properties of magnetite crystals at low temperature, *Phys. Rev.*, 40, 1002-1012.

Medrano, C., M. Schlenker, J. Baruchel, J. Espeso, and Y. Miyamoto (1999), Domains in the low-temperature phase of magnetite from synchrotron-radiation x-ray topographs, *Phys. Rev. B.,* 59, 1185-1195.

Moskowitz, B.M., R.B. Frankel, and D.A. Bazylinski, Rock magnetic criteria for the detection of biogenic magnetite, *Earth Planet. Sci. Lett*., 120, 283-300, 1993.

Muxworthy, A.R., and W. Williams (2006), Low-temperature cooling behavior of single-domain magnetite: Forcing of the crystallographic axes and interactions, *J. Geophys. Res*., 111, B07103, doi:10.1029/2006JB004298.

Özdemir, Ö., and D.J. Dunlop (1996), Thermoremanence and Néel temperature of geothite, *Geophys. Res. Lett*, 23, 912-924.

Özdemir, Ö., D.J. Dunlop, and B.M. Moskowitz, Changes in remanence, coercivity and domain state at low temperature in magnetite, *Earth Planet. Sci. Lett*., 194, 343-358, 2002.

Smirnov, A.V., and J.A. Tarduno (2002), Magnetic field control of the low-temperature magnetic properties of stoichiometric and cation-deficient magnetite, *Earth Planet. Sci. Lett.*, 194, 359-368.

Smirnov, A. V. (2006a), Memory of the magnetic field applied during cooling in the low-temperature phase of magnetite: Grain-size dependence, *J. Geophys. Res*., 111, B12S04, doi:10.1029/2006JB004573.

Smirnov, A. V. (2006b), Low-temperature magnetic properties of magnetite using first-order reversal curve analysis: Implications for the pseudo-single domain state, *Geochem. Geophys. Geosys*., 7, Q11011, doi:10.1029/2006GC001397.

Smirnov, A. V. (2007), Effect of the magnetic field applied during cooling on magnetic hysteresis in the low-temperature phase of magnetite: First-order reversal curve (FORC) analysis, *Geochem. Geophys. Geosys*, 8, Q08005, doi:10.1029/2007GC001650.

Smirnov, A. V. (2009), Grain size dependence of low-temperature remanent magnetization in natural and synthetic magnetite: Experimental study, *Earth Planets Space*, 61, 119-124

Verwey, E.J. (1939), Electronic conduction of magnetite (Fe_3O_4) and its transition point at low temperature, *Nature*, 144, 327-328.

Verwey, E.J., P.W. Haayman, and F.C. Romeijn (1947), Physical properties and cation arrangements of oxides with spinel structure II. Electronic conductivity, *J. Chem. Phys.*, 15, 181-187.

University of Minnesota
291 Shepherd Laboratories
100 Union Street S. E.
Minneapolis, MN 55455-0128
phone: (612) 624-5274
fax: (612) 625-7502
e-mail: irm@umn.edu
www.irm.umn.edu

The IRM Quarterly

The *Institute for Rock Magnetism* is dedicated to providing state-of-the-art facilities and technical expertise free of charge to any interested researcher who applies and is accepted as a Visiting Fellow. Short proposals are accepted semi-annually in spring and fall for work to be done in a 10-day period during the following half year. Shorter, less formal visits are arranged on an individual basis through the Facilities Manager.

The *IRM* staff consists of **Subir Banerjee**, Professor/Founding Director; **Bruce Moskowitz**, Professor/Director; **Joshua Feinberg**, Assistant Professor/Associate Director; **Jim Marvin**, Emeritus Scientist; **Mike Jackson**, **Peat Sølheid**, and **Julie Bowles**, Staff Scientists.

Funding for the *IRM* is provided by the **National Science Foundation**, the **W. M. Keck Foundation**, and the **University of Minnesota**.

The *IRM Quarterly* is published four times a year by the staff of the *IRM*. If you or someone you know would like to be on our mailing list, if you have something you would like to contribute (*e.g.*, titles plus abstracts of papers in press), or if you have any suggestions to improve the newsletter, please notify the editor:

Julie Bowles
Institute for Rock Magnetism
University of Minnesota
291 Shepherd Laboratories
100 Union Street S. E.
Minneapolis, MN 55455-0128
phone: (612) 624-5274
fax: (612) 625-7502
e-mail: jbowles@umn.edu
www.irm.umn.edu

UNIVERSITY OF MINNESOTA

Work at the IRM!

The IRM is hiring a Research Associate or Postdoctoral Associate to assist with facility operations and to carry out original research. Visit the IRM website for more information.

http://www.irm.umn.edu

Review of applications will begin June 30.